Journal of Rock Mechanics and Geotechnical Engineering 16 (2024) 483–496

Contents lists available at ScienceDirect

Journal of Rock Mechanics and Geotechnical Engineering

journal homepage: www.jrmge.cn

Full Length Article

Wetting front migration model of ion-adsorption rare earth during the multi-hole unsaturated liquid injection

Yu Wang [a,b], Xiaojun Wang [a,b,*], Yuchen Qiu [a,b], Hao Wang [a,b], Gang Li [a,b], Kaijian Hu [a,b], Wen Zhong [a,b], Zhongqun Guo [c], Bing Li [a], Chunlei Zhang [a], Guangxiang Ye [d]

[a] Jiangxi Key Laboratory of Mining Engineering, Jiangxi University of Science and Technology, Ganzhou, 341000, China
[b] School of Resources and Environment Engineering, Jiangxi University of Science and Technology, Ganzhou, 341000, China
[c] School of Civil Engineering and Surveying & Mapping Engineering, Jiangxi University of Science and Technology, Ganzhou, 341000, China
[d] Ganzhou Nonferrous Metallurgy Research Institute, Ganzhou, 341000, China

ARTICLE INFO

Article history:
Received 1 December 2022
Received in revised form
9 April 2023
Accepted 15 June 2023
Available online 28 September 2023

Keywords:
Ion-adsorption rare earth ore
Multi-hole unsaturated liquid injection
In situ leaching
Intersection effect
Calculation model

ABSTRACT

In the process of ion-adsorption rare earth ore leaching, the migration characteristics of the wetting front in multi-hole injection holes and the influence of wetting front intersection effect on the migration distance of wetting fronts are still unclear. Besides, wetting front migration distance and leaching time are usually required to optimize the leaching process. In this study, wetting front migration tests of ion-adsorption rare earth ores during the multi-hole fluid injection (the spacing between injection holes was 10 cm, 12 cm and 14 cm) and single-hole fluid injection were completed under the constant water head height. At the pre-intersection stage, the wetting front migration laws of ion-adsorption rare earth ores during the multi-hole fluid injection and single-hole fluid injection were identical. At the post-intersection stage, the intersection accelerated the wetting front migration. By using the Darcy's law, the intersection effect of wetting fronts during the multi-hole liquid injection was transformed into the water head height directly above the intersection. Finally, based on the Green-Ampt model, a wetting front migration model of ion-adsorption rare earth ores during the multi-hole unsaturated liquid injection was established. Error analysis results showed that the proposed model can accurately simulate the infiltration process under experimental conditions. The research results enrich the infiltration law and theory of ion-adsorption rare earth ores during the multi-hole liquid injection, and this study provides a scientific basis for optimizing the liquid injection well pattern parameters of ion-adsorption rare earth in situ leaching in the future.

1. Introduction

Ion-adsorption rare earth ore is one of the important strategic resources related to national security and economic development, and the value of ion-adsorption rare earth has been greatly explored in the economy, national defense industry, and high-tech techniques (Qiu et al., 2014; Luo et al., 2022; Zhou et al., 2022). As indispensable raw materials for the development of high-tech industries (Dushyantha et al., 2020), ion-adsorption rare earth ores are mainly distributed in south China, such as Jiangxi and Fujian provinces. Unlike rare earth minerals in the solid mineral phase, ion-adsorption rare earth elements mostly exist in the form of trivalent cations (Wang et al., 2022). Rare earth carbonate minerals in granite and other parent rocks can be decomposed under long-term weathering (Zhou et al., 2019). With the erosion of rain, the dissolved rare earth elements are adsorbed on the surface of kaolin, halloysite, illite and other clay minerals in the form of rare earth hydrate, and finally enriched in the weathered layer of the mine (Chi et al., 2005). Therefore, the exchange of rare earth cations with more active cations is the only way to extract rare earth elements from ore bodies (Huang et al., 2015, 2021). At present, the in situ leaching method is mainly used for the recovery of rare earth mineral resources. Specifically, without damaging the vegetation on the surface of the mountain, the injection hole is drilled on the mountain surface and the leaching agent ($MgSO_4$ solution) is injected into the injection hole (Xiao et al., 2015; He et al., 2022a);

* Corresponding author. Jiangxi Key Laboratory of Mining Engineering, Jiangxi University of Science and Technology, Ganzhou, 341000, China.
E-mail address: wangxiaojun@jxust.edu.cn (X. Wang).
Peer review under responsibility of Institute of Rock and Soil Mechanics, Chinese Academy of Sciences.

https://doi.org/10.1016/j.jrmge.2023.06.020

the magnesium ions in the solution can desorb the rare earth ions adsorbed on the surface of clay minerals, then rare earth leachate is formed and collected through the liquid collection ditch; finally, the rare earth elements are extracted from the collected rare earth leachate (Nie et al., 2020; Wang et al., 2020; Zhou et al., 2021).

This method avoids the stripping of topsoil, reduces the mining cost, and has significant popularization and application value. Nevertheless, there are two significant problems in the field application of in situ leaching process: (1) Empirical determination of injection well pattern parameters lacks theoretical support. Problems such as "where is the leaching agent extracted" have not been well solved (Wang et al., 2018); and (2) The unsaturated flow law and mechanism of the ion-absorbed rare earth in situ leaching are not sufficiently studied, and the accurate multi-hole fluid injection theory model has not been established. The key link of in situ leaching mining technology is to set well pattern parameters and conduct multi-hole infiltration, while the existing studies mainly focus on the wetting front migration law of ionic rare earth single-hole liquid injection. Guo et al. (2018, 2020) studied the influence law of ion-adsorption rare earth ore particle composition on the migration distance of wetting fronts, and established a model for calculating the influence range of single-hole injection based on the Green-Ampt model. Gui et al. (2018) found that when the well network is infiltrated, the smaller the injection hole spacing, the stronger the interaction between the hole networks. However, only a single-hole injection wetting front migration model was established based on the Philip mode. At present, there is no research on the effect of intersection of multi-hole liquid injection on the migration of wetting front in ion-adsorption rare earth, and only some relevant studies have preliminarily explored the influence law of intersection and infiltration of multi-point sources under different conditions (Li et al., 2017; Fan et al., 2020, 2022). Studies showed that the smaller the spacing between dual point sources, the faster the migration of the wetting front at the intersection interface (Jiang et al., 2022), and that intersection infiltration would increase the NH_4^+-N content of the soil at the intersection interface (He et al., 2022b), but would lead to a decrease in infiltration (Fan et al., 2022). However, the influence law and mechanism of intersection effect are not analyzed comprehensively. Furthermore, the aforementioned studies have all employed drip infiltration without a head height. In contrast, in situ leaching of ion-adsorption rare earth ore involves a head height, leading to a more complex effect of the intersection effect between injection holes on wetting front migration. Therefore, it is necessary to deeply understand and analyze the wetting front migration law of the ion-adsorption rare earth during the multi-hole liquid injection, to explore the influence mechanism of the intersection effect between injection holes on the migration of wetting front.

The infiltration process of the leaching agent into ion-adsorption rare earth ores belongs to unsaturated infiltration (Chen et al., 2022). In recent years, many water infiltration models have been developed to simulate water migration in saturated and unsaturated soils, and model algorithms have been derived to obtain accurate model solutions (Al-Ogaidi et al., 2016; Dang et al., 2020). The existing physical models can be used to describe the infiltration process in detail, among which the Richards model and Green-Ampt model (Green and Ampt, 1911) are the most commonly used models to simulate the infiltration process (Deng and Zhu, 2016; Mao et al., 2016). The solution of the Richards model requires the iterative implicit numerical method, therefore, the calculation process of this model is complex and the calculation amount is large (Rasheed and Sasikumar, 2015). The Green-Ampt model is an analytical solution derived based on the Darcy's law, which has the advantages of simple calculation, high accuracy and clear physical meaning of model parameters. The model presents the assumption of a piston model saturated in the wet zone and was initially applied to soils with uniform, dry, and rough textures. Subsequently, many scholars have made significant improvements (Liu et al., 2021). Therefore, this model has been widely used in various infiltration situations (Yin and Xie, 2016; Liu et al., 2020; Mohammadzadeh-Habili and Khalili, 2021), such as inclined surfaces (Chen and Young, 2006) and layered soils (Ma et al., 2010; Mohammadzadeh-Habili and Heidarpour, 2015). The multi-hole infiltration of ion-adsorption rare earth ore belongs to three-dimensional (3D) unsaturated infiltration, and a wetting area similar to an ellipsoid will be formed under the liquid injection hole. To effectively describe the migration characteristics and influence scope of the wetting body by the Green-Ampt model, the Green-Ampt model was modified from different perspectives (Zhang et al., 2019, 2020). Vigo et al. (2021) established the infiltration models of hemispherical and circular sources based on the Green-Ampt model without considering the depth of surface water. Assuming that the interior of the wetting body is saturated, Guo et al. (2018) established the influence range of single well fluid injection of the ion-adsorption rare earth under the condition of constant water head height based on the conventional Green-Ampt model. Sepaskhah and Chitsaz (2004) proposed an empirical model based on the Green-Ampt model to determine the radius and depth of the wetting front during drip irrigation. Through the Green-Ampt theory, Fei et al. (2019) derived a mathematical model for predicting the shape of the wetting front at a known infiltration rate. Unfortunately, the theoretical models all focus on single-hole injection and do not consider the effect of the intersection between injection holes on the migration of wetting fronts, and there is a large difference between the theoretical study and the real infiltration. Moreover, the Green-Ampt model was applied to ellipsoidal infiltration without correction for two key parameters, hydraulic conductivity and matrix suction, the choice of which will have an impact on the calculation results (Sorensen et al., 2014; Hsu et al., 2017). Therefore, there is an urgent requirement to establish a calculation model for the wetting front migration distance of multi-hole unsaturated liquid injection to provide theoretical guidance for the in situ leaching process.

In this study, the multi-hole liquid injection tests and single-hole liquid injection tests on ion-adsorption rare earth ores under the constant water head height were completed, the differences of wetting front migration between multi-hole liquid injection and single-hole liquid injection were analyzed, and the influence mechanism of intersection on wetting front migration was revealed. The study also improved the piston model assumption of saturation in the wetted zone in the conventional Green-Ampt model, and calculated the unsaturated hydraulic conductivity and matrix suction during ellipsoidal infiltration. The effect of intersection of multi-hole liquid injection on the migration of wetting fronts was considered for the first time, and this effect was quantified based on the Darcy's law. By combining the Green-Ampt model with the intersection effect, a model for the migration of wetting fronts in ion-adsorption rare earth ore with multi-hole unsaturated injection was established. The research results enrich the infiltration law and theory of ion-adsorption rare earth ores during the multi-hole liquid injection. Besides, this study also provides a scientific basis for optimizing the liquid injection well pattern parameters of ion-adsorption rare earth in situ leaching in the future.

2. Test materials and methods

2.1. Test materials

The test sample was taken from an unexploited mine in Dingnan County, Ganzhou City, Jiangxi Province, China, as shown in Fig. 1. The simple geological profile and schematic diagram of in situ leaching for this ion-adsorption rare earth ore are presented in Figs. 2 and 3, respectively. The sampling location was in the completely weathered layer 3 m below the topsoil. The basic physical and chemical indices of undisturbed rare earth samples were tested according to the geotechnical test procedures. The basic physical parameters of the test sample are shown in Table 1.

2.2. Experimental methods

The minimum infiltration unit of multi-hole liquid injection for ion-adsorption rare earth ore was three adjacent liquid injection holes. Considering the influence of dual intersection on the intermediate liquid injection hole, the ore body in the middle part of the dual intersection was taken as the main analysis object. Since the leaching started simultaneously in the three liquid injection holes under the same water head height, the dual intersection surface on both sides was symmetrical about the middle liquid injection hole. Therefore, the area between the intersection surface on either side and the middle liquid injection hole can be studied (Dong et al., 2012). The model equivalence principle is shown in Fig. 4.

Fig. 5 shows the self-designed test device. The length, width and height of the test chamber were 40 cm, 60 cm and 40 cm, respectively, the wall thickness was 1 cm, and the outer wall of the test chamber is labeled with scales. The partition in the figure was the intersection surface (zero flux plane). The water flux on both sides of the zero flux plane was zero, and there was no exchange of liquid volume. Therefore, the acrylic partition can be used to simulate the zero flux plane during the intersection, the spacing of liquid injection holes can be controlled by moving the position of the partition, and the one-way intersection infiltration test and single-hole infiltration test of different liquid injection hole spacings can be completed. The whole test system was composed of an acrylic test chamber, acrylic partition, peristaltic pump, liquid injection hole, overflow hole, measuring cylinder, computer and digital camera.

As the sample was taken from the completely weathered layer of ion-adsorption rare earth ore, the ore sample had a loose structure and poor cohesion, which was easy to be damaged during transportation. Therefore, the original sample was not suitable for preparing standard test samples. To avoid the above defects, remolded samples were taken as the object of this study. The quality of the required ore sample was calculated according to the dry density of rare earth samples and test requirements. The air-dried rare earth samples were loaded into the acrylic test box in three layers using the layered compaction method (Xu et al., 2021). Once the test started, the data were recorded every 10 min, the position of the wetting front directly below the liquid injection hole was recorded through the scale on the acrylic test box to characterize the shape of the wetting front, and the wetting front migration process was photographed. The overflow hole was used to maintain a constant water head height of the liquid injection hole. The actual infiltration amount was calculated by recording the total amount of liquid injection and the amount of water flowing out of the overflow hole, so as to analyze the change in the overall water content of the rare earth sample during the infiltration process.

Fig. 1. Sampling location.

3. Results and discussion

3.1. Migration law of wetting front during the multi-hole liquid injection

The shape change of the wetting front on the wetting profile is the most intuitive embodiment of the migration law of the wetting front during the multi-hole fluid injection. Fig. 6a–c shows the wetting front migration of the ion-adsorption rare earth ores during the multi-hole liquid injection, and Fig. 6d shows the wetting front migration of the ion-adsorption rare earth ores during the single-hole liquid injection. It can be found that at the initial infiltration stage and the pre-intersection stage, the shape of wetting fronts of the multi-hole fluid injection and single-hole fluid injection is the same, which is approximately a quarter ellipse (Zhao et al., 2010). With the progress of infiltration, the wetting front of multi-hole liquid injection migrates to the partition (zero flux plane) and the intersection occurs. On one side of the partition, it is observed that the shape of the wetting area on the intersection surface is a quarter ellipse (Cheng et al., 2007). During continuous liquid injection, the migration distances of the wetting front at the intersection and that directly below the liquid injection hole are becoming closer to the same horizontal line, and the shape of the wetting body gradually evolves from a quarter ellipsoid to a right-angled trapezoid. To facilitate the comparative observation of the shape changes of the wetting front at different spacings, the positions of the wetting front at different periods are depicted in the coordinate system, as shown in Fig. 7. The wetting front migration before and after the intersection during the multi-hole liquid injection is different. Therefore, the multi-hole unsaturated liquid injection of ion-adsorption rare earth ore can be divided into two stages: the pre-intersection stage and the post-intersection stage.

3.2. Intersection effect on the migration distance of wetting front directly below the injection hole

To efficiently determine the well pattern parameters in the actual leaching process, it is necessary to understand the intersection effect on the wetting front migration distance in the infiltration process, and determine the relationship between the influence range of the wetting front during the multi-hole fluid injection and the infiltration time. Among them, the maximum wetting front migration distance $Z_f(t)$ directly below the liquid injection hole is the key parameter of wetting front migration. Fig. 8 summarizes the migration distances $Z_f(t)$ of the wetting front directly below the injection holes of multi-hole and single-hole liquid injection. The comparison results show that at the pre-intersection stage, the migration distances of the wetting front directly below the injection holes of the single-hole and multi-hole liquid injection are the same; at the post-intersection stage, the

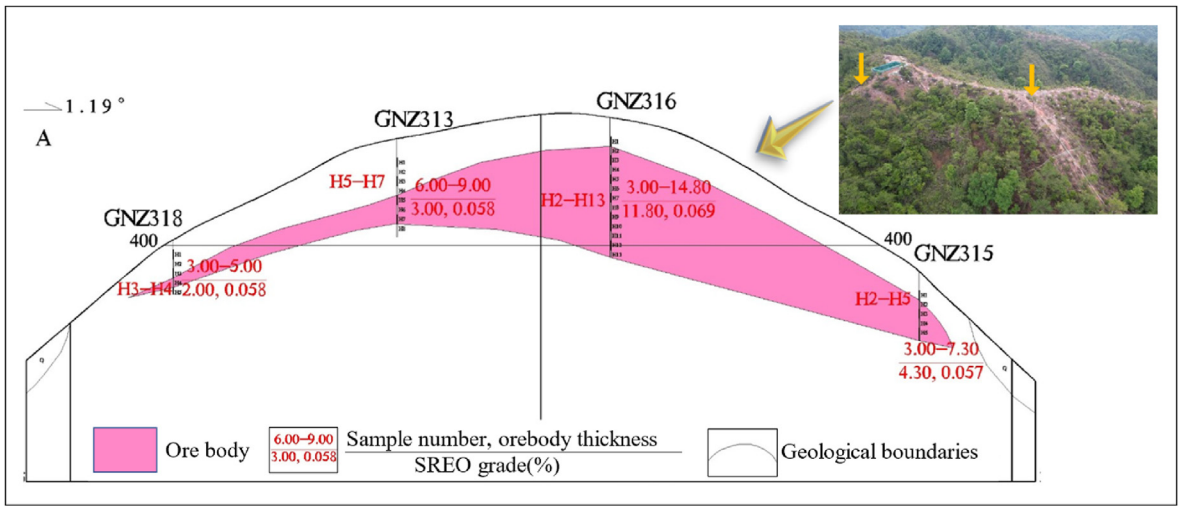

Fig. 2. Geological profile of ion-adsorption rare earth ore.

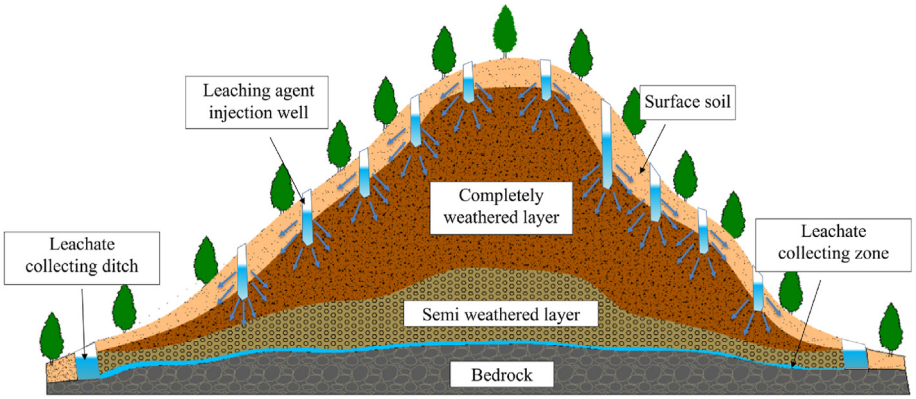

Fig. 3. Schematic diagram of in situ leaching of ion-adsorption rare earth ore.

Table 1
Basic physical parameters of ion-adsorption rare earth samples.

Bulk density (g/cm^3)	Natural water content (%)	Specific gravity	Sand content (%)	Silt content (%)	Clay content (%)
1.32	17	2.62	42.67	51.13	6.2

migration distance of the wetting front directly below the injection hole of multi-hole liquid injection is gradually greater than that of single-hole liquid injection. With the increase in infiltration time, the gap between the two becomes larger and larger. This is can be explained as follows: after the intersection of the wetting front during the multi-hole fluid injection, a zero flux plane is formed at the intersection; there is no exchange of liquid amount on both sides of the zero flux plane (Lei et al., 1988), which hinders the migration of the horizontal wetting front. Therefore, the wetting front can only move vertically downwards along the intersection surface (Yuan et al., 2010). The vertical migration of liquid amount at the intersection increases the water content in the wetting body, which accelerates the wetting front migration directly below the injection hole in the multi-hole fluid injection at the post-intersection stage.

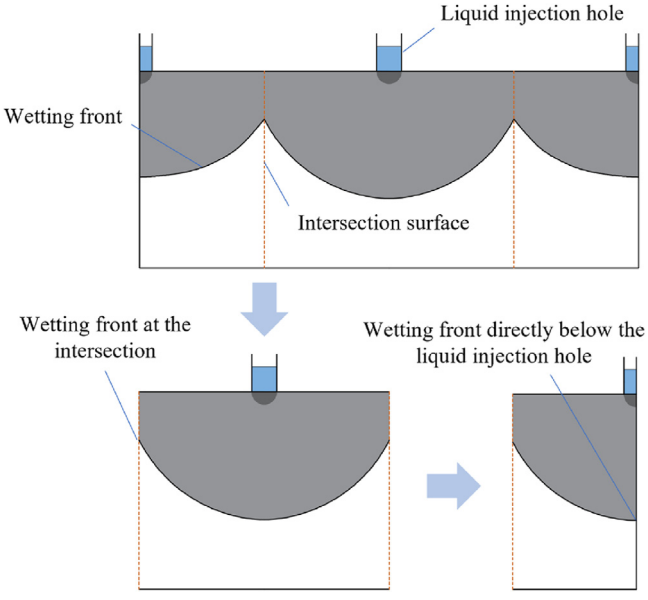

Fig. 4. Model equivalence diagram.

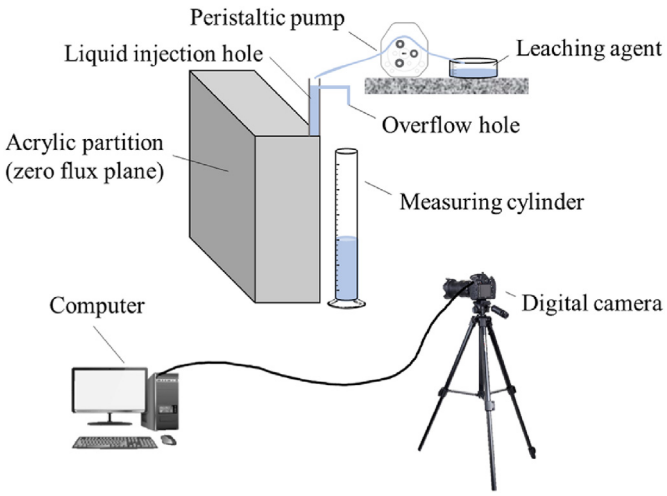

Fig. 5. Test device.

3.3. Intersection effect on water content per unit volume of wetting body

As mentioned in Section 3.2, the intersection of liquid injection holes accelerates the migration of the wetting front directly below the liquid injection holes. Understanding the influence mechanism of intersection is of great significance for establishing the wetting front migration model of the ion-adsorption rare earth during the multi-hole liquid injection. Fig. 9 shows the variation curves of water content per unit volume of the wetting body over time. It can be found that the water content per unit volume of the wetting body at stage I decreases sharply with the infiltration time, regardless of multi-hole or single-hole liquid injection. At stage II, the water content per unit volume of the wetting body decreases slowly with the infiltration time. This is mainly because the volume of the dry ore sample decreases gradually with the increased volume of the wetting body, resulting in a gradual decrease in the overall matrix suction of the soil sample (Hsu et al., 2017); besides, a saturated area is gradually formed below the liquid injection hole (Yao et al., 2019; Zhang et al., 2022), resulting in a slow decrease in the infiltration rate. As a result, the water content per unit volume of the wetting body decreases sharply at first and then slowly during the infiltration process. The water content per unit volume curves of wetting bodies during multi-hole and single-hole liquid injection is compared. It is found that at the pre-intersection stage, the water content per unit volume curves of wetting bodies during the single-hole and multi-hole liquid injection basically coincide. At the post-intersection stage, the water content per unit volume of wetting bodies during the multi-hole liquid injection is greater than that of single-hole liquid injection under the influence of the intersection. At the same infiltration time, the water content per unit volume of wetting bodies increases with the decrease of liquid injection hole spacing. Among them, the water content per unit volume of the wetting body of the single-hole liquid injection is the lowest. It strongly indicates that the intersection of the wetting bodies increases the water content per unit volume of the wetting body during the multi-hole liquid injection, thereby accelerating the migration of the wetting front. Analysis of the wetting front migration pattern and wetting front shape at the intersection interface in Fig. 10 shows that the wetting front at the intersection interface and the single-hole liquid injection wetting front migration pattern are similar, and both have a power function relationship with the infiltration time. Moreover, the shape of the intersection interface is a quarter ellipse, which is exactly similar to the image of the wetting front migration in the single-hole liquid injection. The intersection interface is formed due to the intersection between wetted bodies, and the intersection interface is similar in shape to the single-hole liquid injection wetting peak, indicating that during the process of infiltration, the intersection effect leads to the formation of a hydraulic gradient at the intersection, which will increase the water content per unit volume of the wetted body and thus accelerate the migration of the wetting front. The influence of the intersection effect on the wetting front migration directly below the injection hole is essentially the effect of the hydraulic gradient at the intersection.

4. Theoretical modeling

4.1. Establishment of wetting front migration model at the pre-intersection stage

According to the test results in Section 3.1, the multi-hole liquid injection process of ion-adsorption rare earth can be divided into two stages: the pre-intersection stage and the post-intersection stage of wetting fronts. At the pre-intersection stage, there is no interaction between the injection holes. Thus, the wetting front migration process at the pre-intersection stage of multi-hole unsaturated liquid injection can be described by the wetting front migration model during the single-hole unsaturated liquid injection. At the post-intersection stage, the intersection has an impact on the wetting front migration, and an infiltration model of the multi-hole unsaturated liquid injection considering the intersection effect is required. Firstly, the wetting front migration model at the pre-intersection stage of single-hole unsaturated liquid injection is studied. The single-hole unsaturated liquid injection belongs to a 3D infiltration problem. The liquid injection hole has a constant head height, and the shape of the wetting body below the liquid injection hole is approximately half of an ellipsoid. To study the relationship between wetting front migration distance and infiltration time, the vertical profile of the center of the injection hole is taken for research. All the vertical profiles of the center of the injection hole are the same. At this time, the 3D infiltration problem is transformed into a two-dimensional (2D) infiltration problem. Fig. 11 shows the analysis diagram of the wetting front characteristics during the unsaturated single-hole liquid injection. The radius of the liquid injection hole is defined as r_0, and the water head height of the liquid injection hole is defined as h. With reference to the conventional and the improved Green-Ampt models (Green and Ampt, 1911; Fei et al., 2019), the basic assumptions of this model are as follows: (1) At the beginning of infiltration, the surface water content of the ore sample below the injection hole is saturated; (2) The soil sample is homogeneous; and (3) The water flux from the injection hole to each point on the wetting front is the same.

According to the Green-Ampt model and Darcy's law, the infiltration rate i below the liquid injection hole can be expressed by

$$i = K\frac{h + S_f + Z_f}{L} \tag{1}$$

where K is the hydraulic conductivity; h is the water head height; Z_f is the migration distance of the wetting front directly below the injection hole; S_f is the matrix suction; and L is the distance from any point $(x, 0)$ below the liquid injection hole to (a, b) below the liquid injection hole.

In the in situ leaching process of ion-adsorption rare earth ore, the radius of the liquid injection hole is also an important parameter. When applying a one-dimensional (1D) Green-Ampt infiltration model to 2D infiltration, the radius of the liquid injection hole should be considered. Therefore, if $a>0$, Eq. (1) is integrated to

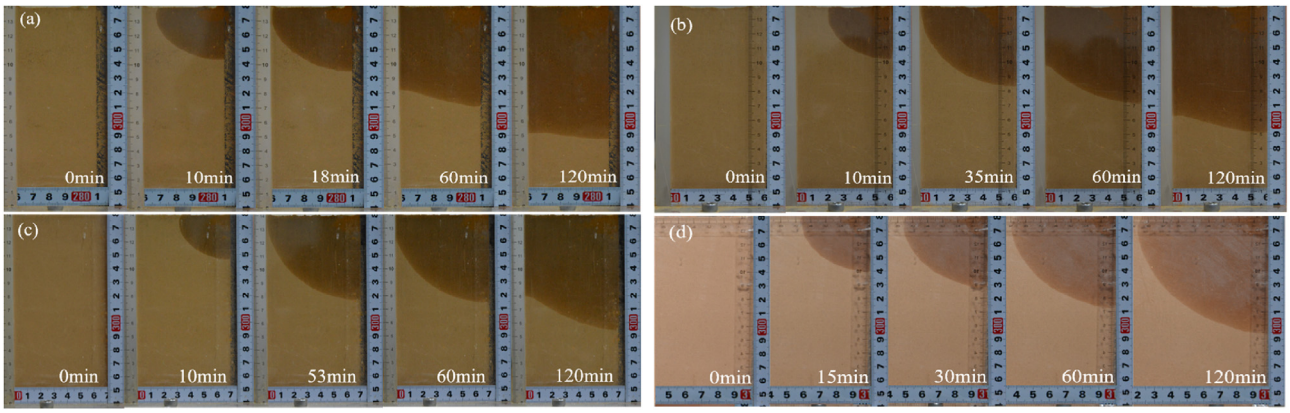

Fig. 6. Measured diagrams of wetting front migration: (a–c) Multi-hole liquid injection at liquid injection hole spacings of 10 cm, 12 cm and 14 cm; and (d) Single-hole liquid injection.

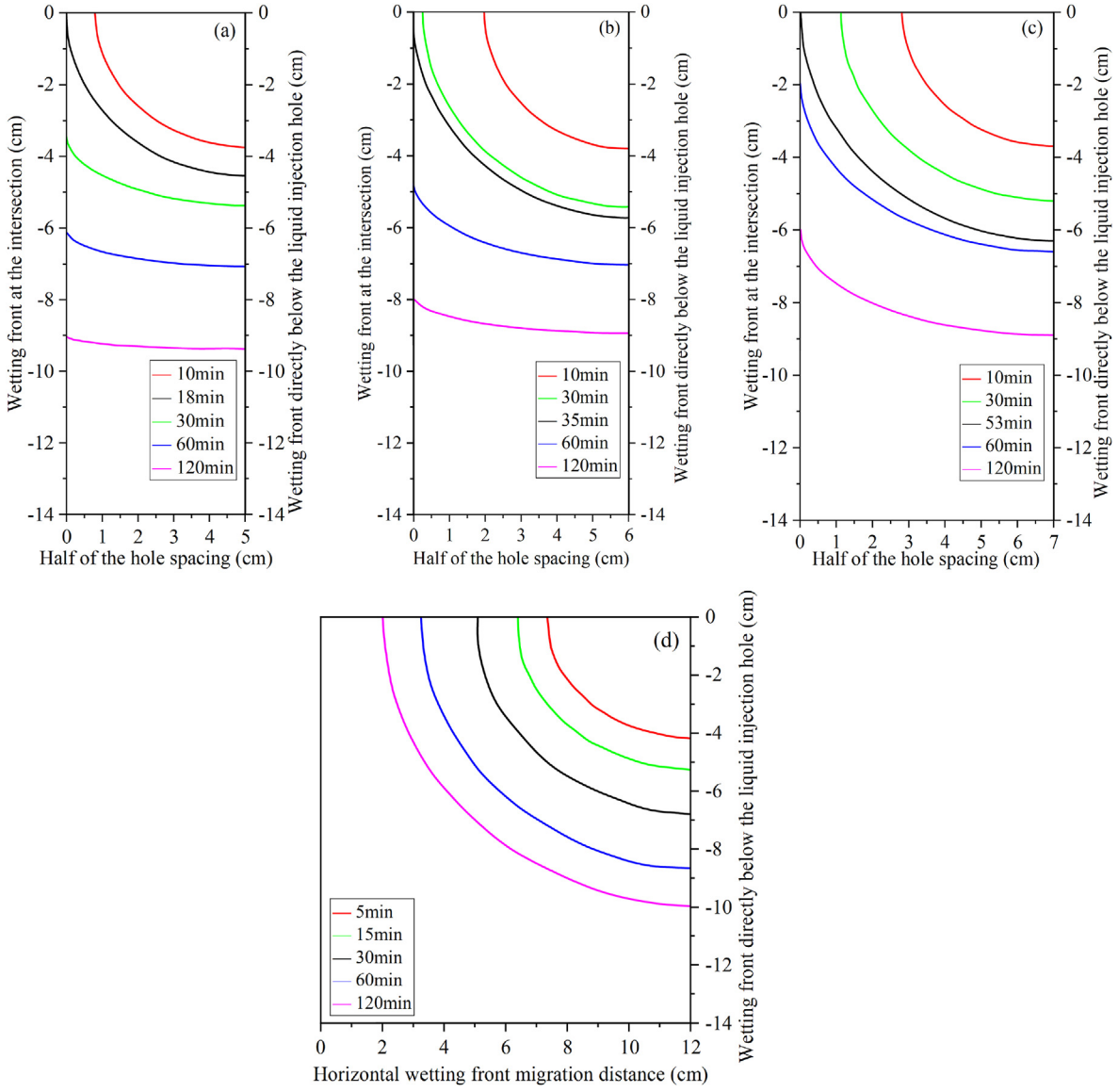

Fig. 7. Results of the wetting front migration: (a–c) Multi-hole liquid injection at liquid injection hole spacings of 10 cm, 12 cm and 14 cm; and (d) Single-hole liquid injection.

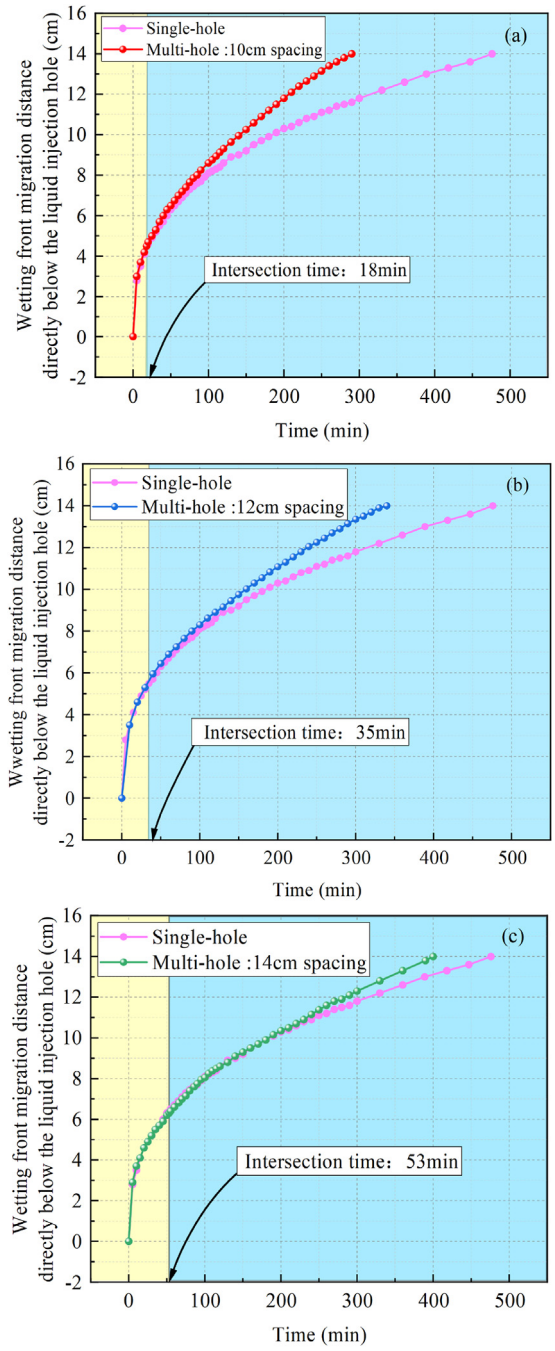

Fig. 8. Relation curves of migration distance and time of wetting front directly below the liquid injection hole: (a) 10 cm spacing, (b) 12 cm spacing, and (c) 14 cm spacing.

obtain the water flux Δq of a single liquid injection hole on one side:

$$\begin{aligned}\Delta q &= \int_{-r_0}^{r_0} K\frac{h+S_f+Z_f}{\sqrt{(a-x)^2+b^2}}\mathrm{d}x \\ &= K\left(h+S_f+Z_f\right)\ln\frac{\sqrt{b^2+(a+r_0)^2}+a+r_0}{\sqrt{b^2+(a+r_0)^2}+a-r_0}\end{aligned} \tag{2}$$

If $a < 0$, Eq. (1) is integrated and the same result is obtained. Thus, the water flux at any point on the wetting front is Δq. As shown in Fig. 11, on the vertical profile, the infiltration length of the liquid injection hole is $2r_0$, the width is the unit width, and the infiltration rate i is the ratio of water flux to its area (only the infiltration source area on the right half of Z-axis is taken here), then the infiltration rate on either side is

$$i = \frac{\Delta q}{r_0} = \frac{K\left(h+S_f+Z_f\right)}{r_0}\ln\frac{\sqrt{b^2+(a+r_0)^2}+a+r_0}{\sqrt{b^2+(a+r_0)^2}+a-r_0} \tag{3}$$

When $a = 0$, $b = Z_f$, the infiltration rate i at any point directly below the injection hole can be obtained as follows:

$$i = \frac{K\left(h+S_f+Z_f\right)}{r_0}\ln\frac{\sqrt{Z_f^2+r_0{}^2}+r_0}{\sqrt{Z_f^2+r_0{}^2}-r_0} \tag{4}$$

In this study, the interior of the wetting body is considered as an unsaturated zone, which is more in line with the actual infiltration situation. In the unsaturated infiltration model, the matrix suction and hydraulic conductivity are two main parameters, which are mainly affected by the water content. Their selection influences the calculation results (Sorensen et al., 2014). Therefore, the distribution law of water content in the wetting front of single-hole unsaturated liquid injection should be determined first. It is found that the distribution of water content in the wetting front of the ion-adsorption rare earth during the single-hole unsaturated liquid injection is similar to that of rare earth samples under 1D vertical infiltration (Peng et al., 2012; Jie et al., 2020). The water content decreases from the center of the injection hole to the surface of the wetting front, and the change rate of the water content increases gradually. It can be seen that the radial position of the wetting front and the change of water content conform to the elliptic curve equation, as shown in Fig. 12.

According to the characteristics of the elliptic curve, the water content at any point in the wetting front meets the elliptic curve equation (Peng et al., 2012). Therefore, the water content at any point x directly below the liquid injection hole is

$$\frac{(\theta-\theta_0)^2}{(\theta_s-\theta_0)^2}+\frac{x^2}{Z_f^2}=1 \tag{5}$$

where θ_s is the saturated water content, θ_0 is the initial water content of the rare earth sample in cm^3/cm^3, x is the distance between a point on the radius of the wetting front and the center of the liquid injection hole, and θ is the water content of the ore sample at the distance x from the point O on the radius of the wetting front.

Therefore, the water content at any point x directly below the liquid injection hole in the wetting front is

$$\theta = (\theta_s-\theta_0)\sqrt{1-\frac{x^2}{Z_f^2}}+\theta_0 \tag{6}$$

However, some researchers found that the soil moisture content cannot reach saturation during unsaturated infiltration and cannot be expressed by the conventional permeability coefficient (Li et al., 2012). Xu et al. (2019) tried to express the soil moisture content in terms of the infiltration coefficient corresponding to the average moisture content of the wet zone, but the results were not accurate. In the proposed unsaturated infiltration model, the relationship between the unsaturated hydraulic conductivity and the internal water content of the wetting body is considered (Brooks and Corey, 1966). The unsaturated hydraulic conductivity in the BC model is used to replace the saturated hydraulic conductivity of the

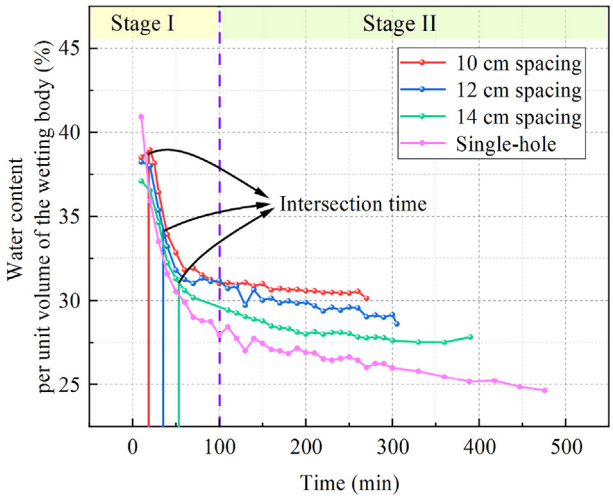

Fig. 9. Relation curves between water content per unit volume and time.

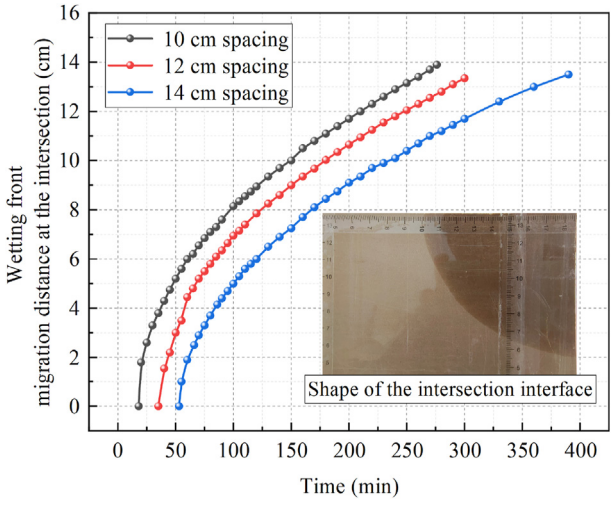

Fig. 10. Relation curves of migration distance and time of the wetting front at the intersection.

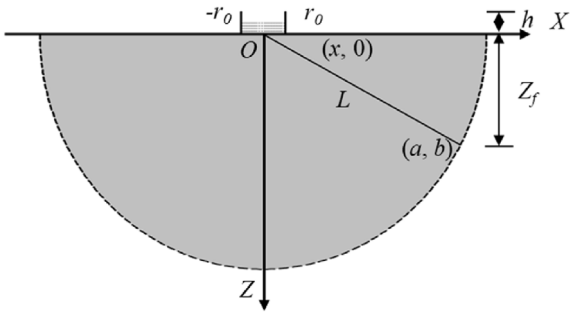

Fig. 11. Analysis of wetting front characteristics during the single-hole unsaturated liquid injection.

conventional Green-Ampt model (Zhang et al., 2020). The derivation process is as follows:

$$K = K_s S_e^{\lambda} \tag{7}$$

$$S_e = \frac{\theta - \theta_r}{\theta_s - \theta_r} \tag{8}$$

$$\lambda = 3 + \frac{2}{\mu} \tag{9}$$

$$\mu = -\frac{\mathrm{d}(\ln S_e)}{\mathrm{d}\left(\ln S_f\right)} \tag{10}$$

where S_e is the effective saturation, θ_r is the residual water content, θ_s is the saturated water content in cm^3/cm^3, μ is the aperture distribution index, λ is a parameter related to the aperture distribution index μ, K is the unsaturated hydraulic conductivity, and K_s is the saturated hydraulic conductivity.

The relationship between the water content of ore samples and matrix suction can be described by the Van Genuchten model (van Genuchten, 1980) as follows:

$$\frac{\theta - \theta_r}{\theta_s - \theta_r} = \frac{1}{\left[1 + \left(\alpha S_f\right)^n\right]^m} \tag{11}$$

where θ_r is the residual water content in cm^3/cm^3; and α, n and m are the optimization parameters of the model.

When Eq. (11) is introduced into Eq. (10), the aperture distribution index can be expressed by

$$\mu = \frac{mn\left(aS_f\right)^n}{1 + \left(aS_f\right)^n} = mn\left(1 - S_e^{1/m}\right) \tag{12}$$

To ensure that the aperture distribution index is single and effective, the effective saturation $S_e = 0.5$ is taken (Lenhard et al., 1989). Therefore, Eq. (12) can be written as follows:

$$\mu = mn\left(1 - 0.5^{1/m}\right) \tag{13}$$

The average hydraulic conductivity of the whole wetting front can be obtained as follows:

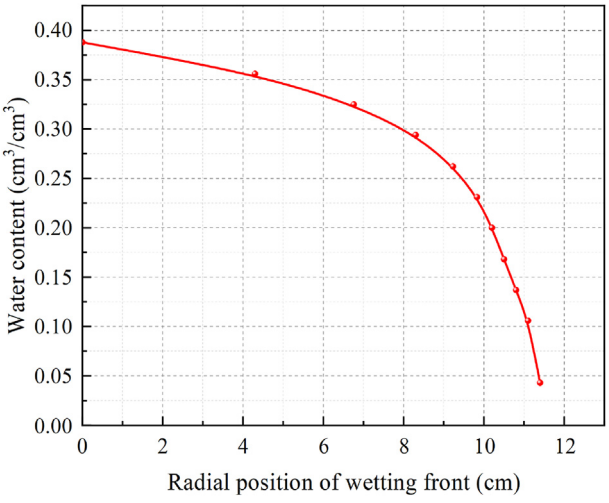

Fig. 12. Relation curve between the radial position of wetting fronts and water content.

$$K = \frac{K_S \iint_S \left(\frac{\theta-\theta_r}{\theta_s-\theta_r}\right)^{\lambda} dS}{S} \tag{14}$$

As expressed in Eqs. (5) and (6), the relationship between the wetting front migration distance and the water content at any point within the wetting front can be described by an elliptic curve. Therefore, by substituting Eq. (6) into Eq. (14), the expression of the unsaturated hydraulic conductivity inside the wetting front can be obtained as follows:

$$K = \frac{K_S \iint_S \left[(\theta_s-\theta_0)\sqrt{1-\frac{x^2}{Z_f^2}}+\theta_0-\theta_r\right]^{\lambda} dS}{S(\theta_s-\theta_r)^{\lambda}} \tag{15}$$

In the infiltration process of the leaching solution, the interior of the wetting body is in an unsaturated state, and the water content of each radius inside the wetting body is different, leading to different matrix suction values. Neuman (1976) studied the effect of the unsaturated wetting body on matrix suction. This method is adopted in this study, and the matrix suction S_f in the wetting body can be expressed as follows:

$$S_f = \int_0^{S_f} k_r dS_f \tag{16}$$

$$k_r = \frac{K}{K_S} \tag{17}$$

where k_r is the relative hydraulic conductivity.

When Eq. (7) is introduced into Eq. (16), the average matrix suction can be obtained:

$$S_f = \int_0^{\frac{1}{a}\left[\left(\frac{\theta_s-\theta_r}{\theta-\theta_r}\right)^{1/m}-1\right]^{1/n}} \frac{1}{\left[1+(aS_f)^n\right]^{m\lambda}} dS_f \tag{18}$$

In this study, the air-dried rare earth sample is used, and its initial water content θ_0 is approximately equal to residual water content θ_r. As shown in Eq. (18), when $\theta_0 = \theta_r$, the initial matrix suction of the rear earth sample is infinite (Zhang et al., 2020). However, the dry rare earth ore sample cannot have an infinite matrix suction, and it is also impossible to have an infinite matrix suction in the leaching process. In addition, there is no convergence in Eq. (18) when the integral upper limit approaches infinity. Therefore, a reasonable value must be selected as the upper limit of the integration of this expression. After multiple integration calculations, when the upper limit of the integration is 10^4–10^7cm, the change of the initial matrix suction of the ore sample has little impact on the overall integration result (Lu and Godt, 2008; Pham et al., 2018). Finally, the initial matrix suction can be set as 10^5 cm, which is a conservative and reasonable value for describing the actual situation.

Table 2
The fitted physical parameters of ore samples.

θ_s (%)	θ_r (%)	m	n	α	K_s (cm/min)
37.35	3.8	0.3584	1.5587	0.0086	0.0374

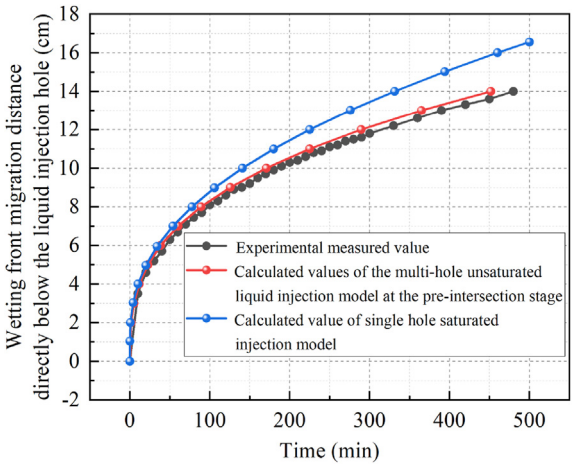

Fig. 13. Comparison of migration distance of the wetting front.

To solve the unsaturated hydraulic conductivity and matrix suction, the soil-water characteristic curve of the ore body is fitted by the RETC software to determine the parameters in the Van Genuchten model, as shown in Table 2.

Matrix suction and hydraulic conductivity are two key parameters of the unsaturated infiltration model. After the above derivation, these parameters can be obtained. Based on the Green-Ampt model and the water balance principle, the relationship between the infiltration amount I and the migration distance of the wetting front Z_f can be obtained at the infiltration time t:

$$I = \iint_{\Omega} \left[(\theta_s-\theta_0)\sqrt{1-\frac{x^2}{Z_f^2}}+\theta_0\right] dS \tag{19}$$

where Ω is the integral area in cm^2, and S is the vertical maximum section area of the wetting body in cm^2.

By differentiating the cumulative infiltration volume with respect to time, the infiltration rate i at any point on the wetting front directly below the liquid injection hole can be written as

$$i = \frac{dI}{dt} = \frac{1}{3}\pi(\theta_s-\theta_0)\frac{dZ_f^2}{dt} = \frac{2}{3}\pi(\theta_s-\theta_0)Z_f\frac{dZ_f}{dt} \tag{20}$$

By combining Eqs. (4) and (20), Eq. (21) can be obtained:

$$\frac{K\left(h+S_f+Z_f\right)}{r_0}\ln\frac{\sqrt{Z_f^2+{r_0}^2}+r_0}{\sqrt{Z_f^2+{r_0}^2}-r_0} = \frac{2}{3}\pi(\theta_s-\theta_0)Z_f\frac{dZ_f}{dt} \tag{21}$$

The migration distance Z_f of the wetting front is integrated on (r_0, Z_f), and the infiltration time t is integrated on (0, t) as follows:

$$\int_{r_0}^{Z_f} \frac{2Z_f}{K\left(h+S_f+Z_f\right)\ln\frac{\sqrt{Z_f^2+{r_0}^2}+r_0}{\sqrt{Z_f^2+{r_0}^2}-r_0}} dZ_f = \int_0^t \frac{3}{\pi(\theta_s-\theta_0)r_0} dt \tag{22}$$

where

$$S_f = \int_0^{\frac{1}{a}\left[\left(\frac{\theta_s-\theta_r}{\theta-\theta_r}\right)^{1/m}-1\right]^{1/n}} \frac{1}{\left[1+(aS_f)^n\right]^{m\lambda}} dS_f$$

$$K = \frac{K_S \iint_S \left[(\theta_s - \theta_0)\sqrt{1 - \frac{x^2}{Z_f^2}} + \theta_0 - \theta_r \right]^{\lambda} dS}{S(\theta_s - \theta_r)^{\lambda}}$$

The Matlab is used to integrate the above equations, and the mathematical relationship between the wetting front migration distance Z_f and time t is calculated. The expression mainly includes the radius of the liquid injection hole r_0, the height of the liquid injection head h, initial water content θ_0, the saturated water content θ_s, the saturated hydraulic conductivity K_s and other parameters. If these parameters are known, the calculation results of the model can be obtained by programming with Matlab software. The measured values of the wetting front migration distance, the calculated values of the wetting front migration distance model at the pre-intersection stage of the multi-hole unsaturated liquid injection and the calculated values of the conventional wetting front migration distance model during the single-hole saturated liquid injection are compared, as shown in Fig. 13. The correlation coefficient between the measured value and the calculated value of the wetting front migration distance at the pre-intersection stage of the multi-hole unsaturated liquid injection is $R^2 = 0.996$. It indicates that the fitting results are good and meet the actual needs of the project. The correlation coefficient between the measured value and the calculated value of the conventional wetting front migration distance model during the single-hole saturated liquid injection is $R^2 = 0.943$. It indicates that the proposed wetting front migration model at the pre-intersection stage of the multi-hole unsaturated liquid injection has a better performance.

To further evaluate the accuracy of the model, the root mean square error (RMSE), percentage of bias (PBIAS) and Nash-Sutcliffe efficiency coefficient (NSE) in statistics are used to evaluate the consistency between the calculated value of the model and the measured value, as expressed in Eqs. (23)–(25), respectively. RMSE reflects the average absolute error of the calculated value and the measured value, PBIAS reflects the relative error of the calculated value and the measured value, and the NSE coefficient reflects the consistency between the calculated value of the model and the measured value over time. The closer the RMSE is to 0 and PBIAS $<$ ±10%, the smaller the difference between the measured value of the test and the calculated value of the model, and the higher the accuracy of the model. The grading standard of the NSE coefficient is as follows: *Excellent* (NSE ≥0.9), *Good* (0.8–0.9), *Acceptable* (0.6–0.8) and *Unsatisfactory* (<0.65) (Ritter and Muñoz-Carpena, 2013). For the wetting front migration model at the pre-intersection stage of the unsaturated multi-hole fluid injection, the RMSE and PBIAS are 0.626 and 5.27%, which are better than the traditional wetting front migration model of single-hole saturated fluid injection (RMSE is 1.29 and PBIAS is 12.26%). The NSE coefficient of the wetting front migration model at the pre-intersection stage of the multi-hole unsaturated liquid injection is 0.938, which is at the level of *Excellent*; while the NSE coefficient of the conventional wetting front migration model during the single-hole saturated liquid injection model is 0.749, which is only in the level of Acceptable. The results show that the proposed model in this study is superior to the conventional model during the single-hole saturated liquid injection.

$$RMSE = \sqrt{\frac{1}{n}\sum_{i=1}^{n}(Z_i - S_i)^2} \tag{23}$$

$$PBIAS = \frac{\sum_{i=1}^{n}(Z_i - S_i)}{\sum_{i=1}^{n} Z_i} \times 100\% \tag{24}$$

$$NSE = 1 - \frac{\sum_{i=1}^{n}(Z_i - S_i)^2}{\sum_{i=1}^{n}(Z_i - M)^2} \tag{25}$$

where Z_i is the measured value of the test at the infiltration time t, S_i is the calculated value of the model at the infiltration time t, M is the average value of the test value, and n is the number of data.

4.2. Establishment of wetting front migration model at the post-intersection stage

After the wetting front of ion-adsorption rare earth during the multi-hole liquid injection intersects, the intersection effect can increase the water content per unit volume in the wetting body. The intersection effect on the water content in the wetting body is converted into the water head height directly above the intersection through Darcy's law. The water head height can change with the variation of the spacing between the injection holes and the infiltration time. The formation of water head height can also increase the water content per unit volume in the wetting body and accelerate the downward migration of the overall wetting front. Based on this, the wetting front migration model at the post-intersection stage of multi-hole unsaturated liquid injection is established in this study. Fig. 14 shows the characteristic analysis of wetting fronts at the post-intersection stage of the multi-hole liquid injection.

As shown in Fig. 14, the intersection is mainly affected by the liquid injection holes on both sides of the intersection surface. The flow q_w of the intersection area can be obtained based on the Darcy's law:

$$q_w = k\frac{2h}{\sqrt{Z_w^2 + b^2}}dA = k\frac{\frac{2hZ_w}{\sqrt{Z_w^2+b^2}}}{Z_w}dA \tag{26}$$

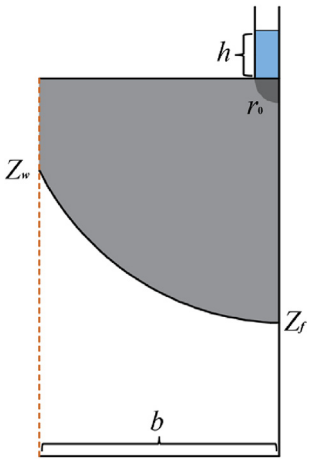

Fig. 14. Characteristic analysis of wetting fronts at the post-intersection stage of the multi-hole liquid injection.

where b is the half distance between injection holes in cm, Z_w is the migration distance of the wetting front at the intersection in cm, h is the water head height of the liquid injection hole in cm, and dA is the area of the liquid injection hole in cm^2.

After the intersection of wetting fronts during the multi-hole liquid injection, the equivalent head height directly above the intersection is h_2:

$$h_2 = \frac{2hZ_w}{\sqrt{Z_w^2 + b^2}} \tag{27}$$

As shown in Fig. 10, after the intersection of wetting fronts during the multi-hole liquid injection, the shape of the intersection surface is quarter elliptical, which is similar to the wetting front migration rule during the single-hole liquid injection. Based on this, the relationship between the migration distance and time of the wetting front at the intersection can be deduced. The migration of the wetting front at the intersection is mainly affected by the equivalent head height h_2. The infiltration rate i_w at the intersection can be obtained through Darcy's law and Green-Ampt model:

$$i_w = K\frac{h + S_f + Z_w}{\sqrt{x^2 + Z_w^2}} \tag{28}$$

Eq. (28) is integrated into the area of liquid injection holes to calculate the infiltration rate i_w at the intersection, and the equivalent head height h_2 is substituted into the equation. Therefore, the infiltration rate i_w at any point directly below the intersection is

$$i_w = \frac{K\left(\frac{2hZ_w}{\sqrt{Z_w^2+b^2}} + S_f + Z_w\right)}{r_0}\ln\frac{\sqrt{Z_w^2 + r_0^2} + r_0}{\sqrt{Z_w^2 + r_0^2} - r_0} \tag{29}$$

Based on the water balance principle and the improved Green-Ampt infiltration model, the cumulative infiltration amount at the intersection can be obtained. The derivative of the cumulative infiltration amount with time can also be used to obtain the infiltration rate i_w at the intersection:

$$i_w = \frac{dI_w}{dt} = \frac{1}{3}\pi(\theta_s - \theta_0)\frac{dZ_w^2}{dt} = \frac{2}{3}\pi(\theta_s - \theta_0)Z_w\frac{dZ_w}{dt} \tag{30}$$

By combining Eqs. (29) and (30), Eq. (31) can be obtained as follows:

$$\frac{K\left(\frac{2hZ_w}{\sqrt{Z_w^2+b^2}} + S_f + Z_w\right)}{r_0}\ln\frac{\sqrt{Z_w^2 + r_0^2} + r_0}{\sqrt{Z_w^2 + r_0^2} - r_0} = \frac{2}{3}\pi(\theta_s - \theta_0)Z_w\frac{dZ_w}{dt} \tag{31}$$

Eq. (32) can be obtained by simplifying Eq. (31):

$$\int_{r_0}^{Z_w}\frac{2Z_w}{K\left(\frac{2hZ_w}{\sqrt{Z_w^2+b^2}} + S_f + Z_w\right)\ln\frac{\sqrt{Z_w^2+r_0^2}+r_0}{\sqrt{Z_w^2+r_0^2}-r_0}}dZ_w = \int_0^t \frac{3}{\pi(\theta_s - \theta_0)r_0}dt \tag{32}$$

Due to the influence of the intersection, the equivalent water head height that changes with the location of the wetting front at the intersection is formed directly above the intersection, and this equivalent water head height also accelerates the migration of the wetting front directly below the liquid injection hole. The intersection is affected by the liquid injection holes on both sides, according to the Darcy's law, the flow q_f at the wetting front directly below the injection hole can be obtained:

$$q_f = k\frac{h}{Z_f}dA + k\frac{\frac{4hZ_w}{\sqrt{Z_w^2+b^2}}}{\sqrt{Z_f^2+b^2}}dA = k\frac{h + \frac{4hZ_fZ_w}{\sqrt{(Z_f^2+b^2)(Z_w^2+b^2)}}}{Z_f}dA \tag{33}$$

Therefore, the equivalent water head height H directly above the liquid injection hole is obtained:

$$H = h + \frac{4hZ_fZ_w}{\sqrt{\left(Z_f^2 + b^2\right)\left(Z_w^2 + b^2\right)}} \tag{34}$$

Fig. 15 shows the equivalent model.

So far, the influence of intersection on the wetting front directly below the liquid injection hole is transformed into the influence of variable water head height of a single-hole on the wetting front directly below the liquid injection hole. After obtaining the expression of equivalent water head height directly above the liquid injection hole, according to the Green-Ampt model and Darcy's law, the migration model of the wetting front directly below the liquid injection hole is expressed as follows:

$$\int_{r_0}^{Z_f}\frac{2Z_f}{K\left[h + \frac{4hZ_fZ_w}{\sqrt{(Z_f^2+b^2)(Z_w^2+b^2)}} + \overline{S_f} + Z_f\right]\frac{\sqrt{Z_f^2+r_0^2}+r_0}{\sqrt{Z_f^2+r_0^2}-r_0}}dZ_f = \int_0^T\frac{3}{\pi(\theta_s - \theta_0)r_0}dt \tag{35}$$

where

$$T = t + t_0$$

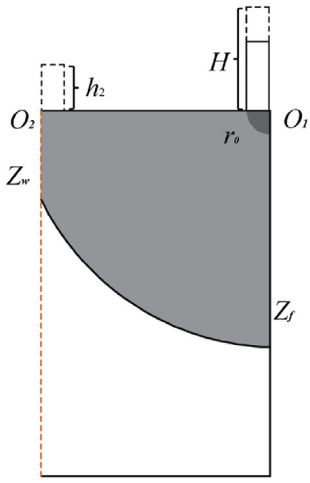

Fig. 15. Model diagram of water head height directly above the liquid injection hole.

$$S_f = \int_0^{\frac{1}{a}\left[\left(\frac{\theta_s-\theta_r}{\theta-\theta_r}\right)^{1/m}-1\right]^{1/n}} \frac{1}{\left[1+\left(aS_f\right)^n\right]^{m\lambda}} dS_f$$

$$K = \frac{K_S \iint_S \left[(\theta_s-\theta_0)\sqrt{1-\frac{x^2}{Z_f^2}}+\theta_0-\theta_r\right]^{\lambda} dS}{S(\theta_s-\theta_r)^{\lambda}}$$

where T is the infiltration time in min, t_0 is the intersection time in min, and t is the migration time of the wetting front at the intersection in min.

Eq. (32) can be used to calculate Z_w at time t, which can be substituted into Eq. (35) to obtain Z_f at time T. The measured values of the wetting front migration distance directly below the liquid injection hole are compared with the calculated values of the model at different liquid injection hole spacing. As shown in Fig. 16, the correlation coefficients R^2 are above 0.97, indicating that there are good fitting results. The PBIAS is less than 6%, NSE coefficients are greater than 0.91, and the classification is above the level of *Excellent*. It indicates that the model has a good fitting performance. As shown in Fig. 16, the measured values are generally lower than the calculated values of the model. This is mainly because the intersection effect is a cumulative process, while the calculated values of the model are instantaneous, which leads to the larger model calculation results. Besides, the larger the liquid injection hole spacing, the less significant the intersection effect at the initial intersection stage. With the increase of infiltration time, the intersection effect increases, and the error rate of the proposed model gradually decreases.

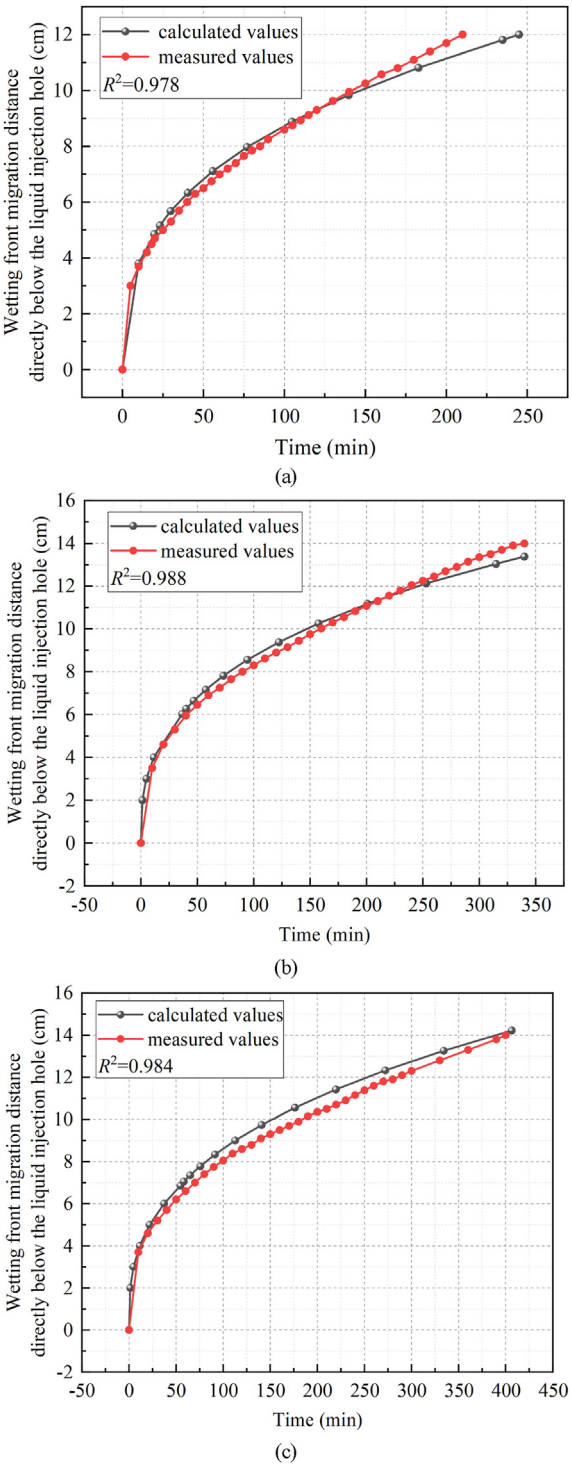

Fig. 16. Calculated and measured values of wetting fronts directly below the liquid injection hole: (a) 10 cm spacing, (b) 12 cm spacing, and (c) 14 cm spacing.

5. Conclusions

In this study, the intersection effect of the wetting front of ion-adsorption rare earth ores during the multi-hole unsaturated liquid injection on the infiltration process is analyzed, as well as its influence mechanism. Based on the Green-Ampt model, the wetting front migration model of ion-adsorption rare earth ore during the multi-hole unsaturated liquid injection is established. The main conclusions are drawn as follows:

(1) The infiltration process of the multi-hole fluid injection for ion-adsorption rare earth ores can be divided into two stages: the pre-intersection stage and the post-intersection stage. At the pre-intersection stage, the shape of the wetting front is a quarter ellipse, and the wetting front migration law of the multi-hole fluid injection is consistent with that of the single-hole fluid injection. At the post-intersection stage, the zero flux plane is formed at the intersection, which accelerates the migration of the wetting front under the injection hole. The shape of the wetting front is approximately a right-angled trapezoid.

(2) The water content per unit volume in the wetting body during the infiltration process of multi-hole fluid injection and single-hole fluid injection is calculated. It is found that the water content per unit volume of the wetting body during the multi-hole fluid injection is greater than that of the single-hole fluid injection. It indicates that the intersection of the wetting fronts during the multi-hole fluid injection can increase the water content per unit volume of the wetting body, thereby accelerating the overall wetting front migration.

(3) The wetting front migration law and wetting front shape at the intersection interface are similar to that during the single-hole injection. Therefore, there is a virtual head height directly above the intersection, which is mainly due to the accumulation and vertical migration of liquid volume at the intersection interface (zero flux plane). Based on this, the

influence of intersection on the wetting front migration can be transformed into the influence of virtual head height.

(4) Based on the law of mass conservation and the Green-Ampt infiltration model, the wetting front migration model of ion-adsorption rare earth ores at the pre-intersection and post-intersection stages of the multi-hole unsaturated liquid injection is derived. The calculated values of the proposed model are consistent with measured values, with a high degree of coincidence. Therefore, the proposed model can better predict the influence range and infiltration rate of the wetting body under the condition of multi-hole liquid injection.

Declaration of competing interest

The authors declare that they have no known competing financial interests or personal relationships that could have appeared to influence the work reported in this paper.

Acknowledgments

This research was funded by the National Natural Science Foundation of China (Grant No. 52174113), the Young Jinggang Scholars Award Program in Jiangxi Province, China (Grant No. QNJG2018051), the “Thousand Talents” of Jiangxi Province, China (Grant No. jxsq2019201043).

References

Al-Ogaidi, A.A.M., Wayayok, A., Rowshon, M.K., Abdullah, A.F., 2016. Wetting patterns estimation under drip irrigation systems using an enhanced empirical model. Agric. Water Manag. 176, 203–213.
Brooks, R.H., Corey, M.A., 1966. Properties of porous media affecting fluid flow. J. Irrigat. Drain. Eng. 92 (2), 61–88.
Chen, L., Young, M.H., 2006. Green-Ampt infiltration model for sloping surfaces. Water Resour. Res. 42 (7), 274–282.
Chen, Y.F., Ye, Y.K., Hu, R., Yang, Z.B., Zhou, C.B., 2022. Modeling unsaturated flow in fractured rocks with scaling relationships between hydraulic parameters. J. Rock Mech. Geotech. Eng. 14, 1697–1709.
Chi, R.A., Tian, J., Li, Z.J., Peng, C., Wu, Y.X., Li, S.R., Wang, C.W., Zhou, Z.A., 2005. Existing state and partitioning of rare earth on weathered ores. J. Rare Earths 23 (6), 756–759.
Cheng, D.J., Fei, L.J., Yin, J., 2007. Reduction volume and interference interface area under film hole unilateral interference infiltration. Trans. Chin. Soc. Agric. Eng. 23 (6), 105–108.
Dang, M.R., Chai, J.R., Xu, Z.G., Qin, Y., Cao, J., Liu, F.Y., 2020. Soil water characteristic curve test and saturated-unsaturated seepage analysis in Jiangcungou municipal solid waste landfill. China Eng. Geol. 264, 105374.
Deng, P., Zhu, J.T., 2016. Analysis of effective Green-Ampt hydraulic parameters for vertically layered soils. J. Hydrol. 538, 705–712.
Dong, Y.Y., Fei, L.J., Mu, H.W., 2012. Mathematical models for single-line interference infiltration of fertilizer solution in film hole. Agric. Res. Arid Areas 30 (3), 81–84.
Dushyantha, N., Batapola, N., Ilankoon, I.M.S.K., Rohitha, S., Premasiri, R., Abeysinghe, B., Ratnayake, N., Dissanayake, K., 2020. The story of rare earth elements (REEs): occurrences, global distribution, genesis, geology, mineralogy and global production. Ore Geol. Rev. 122, 103521.
Fan, Y.W., Shao, X.X., Gong, J.G., Wang, Y., 2020. An empirical model for estimating soil wetting pattern dimensions during film hole irrigation. Arch. Agron Soil Sci. 66 (13), 1765–1779.
Fan, Y.W., Shi, W., Shao, X.X., Zhang, C.Y., Yin, W.F., 2022. Infiltration reduction characteristics and a simplified calculation model of film hole irrigation during interference infiltration. Irrigat. Drain. 71 (1), 35–47.
Fei, L.J., Kang, S.X., Nie, W.B., Zhong, Y., Jiang, R.R., 2019. Development and verification of 3D Green-Ampt based membrane pore infiltration model. Trans. Chin. Soc. Agric. Eng. 35 (21), 69–75.
Green, W.H., Ampt, G.A., 1911. Studies on soil physics: 1. Flow of air and water through soils. J. Agric. Sci. 4, 1–24.
Gui, Y., Wang, G.S., Lai, Y.M., Hong, B.G., Hu, S.L., Long, P., 2018. A calculation model of influence radius of single-hole injection in in situ leaching. Chinese J. Nonferrous Met. 28 (5), 1050–1058.
Guo, Z.Q., Lai, Y.M., Jin, J.F., Zhou, J.R., Zhao, K., Zheng, S., 2020. Effect of particle size and grain composition on two-dimensional infiltration process of weathered crust elution-deposited rare earth ores. Trans. Nonferrous Metals Soc. China 30 (6), 1647–1661.
Guo, Z.Q., Lai, Y.M., Zhao, K., Jin, J.F., Wang, G.S., 2018. Influence range of single hole injection of ionic rare earth for constant head. Chin. J. Nonferrous Metals 28 (9), 1918–1927 (in Chinese).
He, Q., Qiu, J., Chen, J.F., Zan, M.M., Xiao, Y.F., 2022a. Progress in green and efficient enrichment of rare earth from leaching liquor of ion adsorption type rare earth ores. J. Rare Earths 40 (3), 353–364.
He, Z.J., Shi, T.L., Fu, Y.L., Fei, L.J., 2022b. Effect of emitter spacing on nitrogen transport characteristics of intersecting two point sources in bubbled-root irrigation. J. Agric. Sci. Technol. 24 (5), 157–169.
Hsu, S.Y., Huang, V., Park, S.W., Hilpert, M., 2017. Water infiltration into prewetted porous media: dynamic capillary pressure and Green-Ampt modeling. Adv. Water Resour. 106, 60–67.
Huang, X.W., Long, Z.Q., Wang, L.S., Feng, Z.Y., 2015. Technology development for rare earth cleaner hydrometallurgy in China. Rare Met. 34 (4), 215–222.
Huang, S.X., Feng, J., Yu, J.X., Wang, Y., Liu, J.Q., Chi, R.A., Hou, H.B., 2021. Adsorption and desorption performances of ammonium on the weathered crust elution-deposited rare earth ore. Colloids Surfaces A Physicochem. Eng. Asp. 613, 126139.
Jiang, R.R., Fei, L.J., Kang, S.X., 2022. Numerical study on the characteristics of multi-point interference infiltration wetted body in muddy water film hole irrigation. J. Soil Water Conserv. 36 (4), 190–195.
Jie, F.L., Fei, L.J., Zhong, Y., Liu, L.H., Kang, S.X., 2020. Effect of initial soil water content on wetting body characteristics of film hole irrigation. Trans. Chin. Soc. Agric. Eng. 36 (14), 174–181.
Lei, Z.D., Yang, S.X., Xie, S.C., 1988. Fixed plane flux method and its application to soil water balance. J. Hydraul. Eng. 114 (5), 1–7.
Lenhard, R.J., Parker, J.C., Mishra, S., 1989. On the correspondence between brooks-corey and van Genuchten models. J. Irrigat. Drain. Eng. 115 (4), 744–751.
Li, N., Xu, J.C., Qin, Y.Z., 2012. Research on calculation model for stability evaluation of rainfall-induced shallow landslides. Rock Soil Mech. 33 (5), 1485–1490.
Li, Y.B., Fan, Y.W., Liu, Y., Ma, X.Y., 2017. Influencing factors and simplified model of film hole irrigation. Water 9 (7), 543.
Liu, G.G., Li, S.H., Wang, J.X., 2021. New Green-Ampt model based on fractional derivative and its application in 3D slope stability analysis. J. Hydrol. (Amst.) 603, 127084.
Liu, Z.Z., Yan, Z.X., Qiu, Z.H., Wang, X.G., Li, J.W., 2020. Stability analysis of an unsaturated soil slope considering rainfall infiltration based on the Green-Ampt model. J. Mt. Sci. 17 (10), 2577–2590.
Lu, N., Godt, J., 2008. Infinite slope stability under steady unsaturated seepage conditions. Water Resour. Res. 44 (11).
Luo, X.P., Zhang, Y.B., Zhou, H.P., He, K.Z., Zhang, B.Y., Zhang, D.M., Xiao, W.J., 2022. Pore structure characterization and seepage analysis of ionic rare earth ore-bodies based on computed tomography images. Int. J. Min. Sci. Technol. 32 (2), 411–421.
Ma, Y., Feng, S.Y., Su, D.Y., Gao, G.Y., Huo, Z.L., 2010. Modeling water infiltration in a large layered soil column with a modified Green–Ampt model and HYDRUS-1D. Comput. Electron. Agric. 71, S40–S47.
Mao, L.L., Li, Y.Z., Hao, W.P., Zhou, X.N., Xu, C.Y., Lei, T.W., 2016. A new method to estimate soil water infiltration based on a modified Green-Ampt model. Soil Tillage Res. 161, 31–37.
Mohammadzadeh-Habili, J., Heidarpour, M., 2015. Application of the Green–Ampt model for infiltration into layered soils. J. Hydrol. (Amst.) 527, 824–832.
Mohammadzadeh-Habili, J., Khalili, D., 2021. Development of the green-ampt infiltration rate model and relationship of the GA model parameters with soil hydraulic parameters. J. Hydrol. Eng. 26 (11).
Neuman, S.P., 1976. Wetting front pressure head in the infiltration model of Green and Ampt. Water Resour. Res. 12 (3), 564–566.
Nie, W.R., Zhang, R., He, Z.Y., Zhou, J., Wu, M., Xu, Z.G., Chi, R.A., Yang, H.F., 2020. Research progress on leaching technology and theory of weathered crust elution-deposited rare earth ore. Hydrometallurgy 193, 105295.
Peng, Z.Y., Huang, J.S., Wu, J.W., Guo, H., 2012. Modification of Green-Ampt model based on the stratification hypothesis. Adv. Water Sci. 23 (1), 59–66.
Pham, K., Kim, D., Choi, H.J., Lee, I.M., Choi, H., 2018. A numerical framework for infinite slope stability analysis under transient unsaturated seepage conditions. Eng. Geol. 243, 36–49.
Qiu, T.S., Fang, X.H., Wu, H.Q., Zeng, Q.H., Zhu, D.M., 2014. Leaching behaviors of iron and aluminum elements of ion-absorbed-rare-earth ore with a new impurity depressant. Trans. Nonferrous Metals Soc. China 24 (9), 2986–2990.
Rasheed, S., Sasikumar, K., 2015. Modelling vertical infiltration in an unsaturated porous media using Neural network architecture. Aquat. Proc. 4, 1008–1015.
Ritter, A., Muñoz-Carpena, R., 2013. Performance evaluation of hydrological models: statistical significance for reducing subjectivity in goodness-of-fit assessments. J. Hydrol. 480, 33–45.
Sepaskhah, A.R., Chitsaz, H., 2004. Validating the Green-Ampt analysis of wetted radius and depth in trickle irrigation. Biosyst. Eng. 89 (2), 231–236.
Sorensen, J.P.R., Finch, J.W., Ireson, A.M., Jackson, C.R., 2014. Comparison of varied complexity models simulating recharge at the field scale. Hydrol. Process. 28 (4), 2091–2102.
Van Genuchten, M.T., 1980. A closed-form equation for predicting the hydraulic conductivity of unsaturated soils. Soil Sci. Soc. Am. J. 44 (5), 892–898.
Vigo, Á. del, Zubelzu, S., Juana, L., 2021. Infiltration models and soil characterisation for hemispherical and disc sources based on Green-Ampt assumptions. J. Hydrol. 595, 125966.

Wang, G.S., Lai, Y.M., Long, P., Hu, S.L., Hong, B.G., Gui, Y., 2018. Calculation moisture content distribution around injection hole during in situ leaching process of ion-adsorption rare earth mines. Chin. J. Geotech. Eng. 40 (45), 910–917.
Wang, G.F., Xu, J., Ling, Y.R., et al., 2022. A green and efficient technology to recover rare earth elements from weathering crusts. Nat. Sustain.
Wang, X.J., Wang, H., Sui, C., Zhou, L.B., Feng, X., Huang, C.G., Zhao, K., Zhong, W., Hu, K.J., 2020. Permeability and adsorption–desorption behavior of rare earth in laboratory leaching tests. Minerals 10 (10), 1–15.
Xiao, Y.F., Chen, Y.Y., Feng, Z.Y., Huang, X.W., Huang, L., Long, Z.Q., Cui, D.L., 2015. Leaching characteristics of ion-adsorption type rare earths ore with magnesium sulfate. Trans. Nonferrous Metals Soc. China 25 (11), 3784–3790.
Xu, P.P., Zhang, Q.Y., Qian, H., Guo, M., Yang, F.X., 2021. Exploring the geochemical mechanism for the saturated permeability change of remolded loess. Eng. Geol. 284, 105927.
Xu, X., Xi, Y., Yao, W.J., 2019. Unsaturated wetting front model based on the whole process of rainfall infiltration. J. Hydraul. Eng. 50 (9), 1095–1102.
Yao, W.N., Li, C.D., Zhan, H.B., Zeng, J.B., 2019. Time-dependent slope stability during intense rainfall with stratified soil water content. Bull. Eng. Geol. Environ. 78 (7), 4805–4819.
Yin, S.H., Xie, F.F., 2016. Infiltration head of ion-absorbed rare earth with column leaching experiment determined based on Green-Ampt model. Chinese J. Nonferrous Met. 26 (12), 2668–2675.
Yuan, C.F., Li, M.S., Yu, Y.L., Li, X.L., 2010. Effects of drippers spacing on soil moisture uniformity under linear source drip irrigation. J. Shihezi Univ. Sci. 28 (4), 492–496.
Zhang, Q.Y., Chen, W.W., Kong, Y.Z., 2020. Modification and discussion of the Green-Ampt model for an evolving wetting profile. Hydrol. Sci. J. 65 (12), 2072–2082.
Zhang, Q.Y., Chen, W.W., Zhang, Y.M., 2019. Modification and evaluation of Green–Ampt model: dynamic capillary pressure and broken-line wetting profile. J. Hydrol. 575, 1123–1132.
Zhang, Z.G., Lv, X.L., Mao, M.D., Pan, Y.T., Fang, L., Wu, Z.T., 2022. Mechanical response for rainfall-induced landslides on jointed gas pipelines. Comput. Geotech. 146, 104708.
Zhao, W.X., Zhang, Z.H., Cai, H.J., Xie, H.X., 2010. Improvement and verification of the Green-Ampt model for constant-head well permeameter. J. Hydraul. Eng. 41 (4), 464–470.
Zhou, F., Liu, Q., Feng, J., Su, J.X., Liu, X., Chi, R.A., 2019. Role of initial moisture content on the leaching process of weathered crust elution-deposited rare earth ores. Sep. Purif. Technol. 217 (15), 24–30.
Zhou, H.P., Xie, F.X., Zhang, Y.B., Luo, X.P., 2022. Geochemical characteristics and physical properties of ion adsorption type rare earth ore. Chin. J. Rare Met. 46 (1), 78–86.
Zhou, L.B., Wang, X.J., Huang, C.G., Wang, H., Ye, H.C., Hu, K.J., Zhong, W., 2021. Development of pore structure characteristics of a weathered crust elution-deposited rare earth ore during leaching with different valence cations. Hydrometallurgy 201, 105579.

Xiaojun Wang obtained his Master's degree in Mining Engineering from Jiangxi University of Science and Technology, China, in 2006 and his PhD in Engineering Mechanics from Beijing University of Science and Technology, China, in 2012. He was the associate professor in the Department of Mining Engineering at Jiangxi University of Science and Technology, China from 2013 to 2017, and was promoted to professor at the Key Laboratory of Mining Engineering in Jiangxi Province since 2017. His research interests include (1) efficient seepage and disaster prevention of ion-adsorption rare earth; (2) green and efficient mining of metal mines; and (3) analysis of rock mass stability in mines.